ORIGINAL RESEARCH ARTICLE

Dielectric Properties and Magnetodielectric Effect of $Co_{1-x}Cr_xFe_2O_4$

M. A. Islam[1] · A. K. M. Akther Hossain[1] (ORCID)

Abstract

This research investigates the dielectric and magnetodielectric properties of spinel-type Cr^{3+}-substituted cobalt ferrites with the general formula $Co_{1-x}Cr_xFe_2O_4$ ($x = 0.000, 0.125, 0.250, 0.375, 0.500$) over a wide range of temperatures and frequencies. The samples are synthesized by solid-state reaction via ball milling for 12 h and sintering at 1200°C. The grain size estimated from scanning electron microscopic images shows a decreasing value with increased Cr^{3+} content. The compactness of grain size reduces the dielectric behavior as analyzed from the frequency-dependent complex permittivity. The temperature-dependent real permittivity reveals that the $x = 0.125, 0.250$, and 0.375 samples behave as relaxor ferroelectric compounds, whereas the $x = 0$ and 0.5 samples behave as diffuse ferroelectrics. Detailed analysis of the electric modulus from the complex permittivity reveals the grain boundary and grain contribution, respectively. Around the relaxation frequency, a notable magnetodielectric response (maximum 6.5%, in the presence of 1 T applied magnetic field at room temperature) is found for all samples.

Keywords Ferrite · permittivity · magnetodielectric effect

Introduction

In contemporary technology and the biomedical field, AB_2O_4-type spinel ferrites are valued for their affordability and cost-effectiveness in electrical and magnetic sensing applications.[1–8] There are a variety of ferrites; among them, cobalt ferrite (CFO) has become the main focus of intensive research over the decades. This is because of the wide variety of total solid solutions that can be achieved with CFO by doping using transition or rare-earth elements that exhibit tuned and tailored physical properties. It is very interesting to study the effect of dopant/substituent on the magnetic and electric properties of the CFO system for fundamental research to broaden the idea of the physical mechanism behind the cause. Numerous research teams have investigated the effects of substituting various divalent or trivalent cations with cobalt ferrite on its various physical and chemical properties.[6,9–14] Substitution of Bi^{3+}, Al^{3+}, Mn^{2+}, Ni^{2+}, and Zn^{2+} on the Co sites of CFO improves the magnetic and dielectric behavior.[15] Because of

the Cr^{3+} substitution, there is a reduction in the saturation magnetization and coercivity in CFO.[16,17] In addition, Cr^{3+} substitution also affects the dielectric properties in CFO.[17] Cr^{3+} substitution in place of Co^{2+} affects the magnetic and dielectric properties in CFO.[18,19] Impedance spectroscopy is utilized to study the AC electrical properties, providing valuable insights into conduction phenomena in ferrites based on localized electrical charge carriers.[20] These properties can be tuned by suitable substitutions of divalent/trivalent cations in A-site or B-site cations in the spinel structure.[20–25] Various researchers have investigated the effect of frequency, temperature, and substitution on CFO and have found exciting behavior.[20–25]

The dielectric properties are of great importance for ferrites, not only from the application point of view but also from a fundamental perspective. The polycrystalline material exhibits dielectric behavior due to the contribution of interfacial and hopping polarization. Lahouli et al.[8] studied the frequency-dependent permittivity as a function of frequency for Ni-Zn-Al ferrites. Kumar et al.[24] studied the frequency-dependent dielectric properties of Ni-doped cobalt ferrite. Recently, the effect of temperature on dielectric properties has been found where the para-ferroelectric phase transition and the nature of ferroelectrics can be determined. Tiwari et al.[26] studied dielectric permittivity as a function of the

✉ A. K. M. Akther Hossain
akmhossain@phy.buet.ac.bd

1 Department of Physics, Bangladesh University of Engineering and Technology, Dhaka 1000, Bangladesh

temperature of $Ba_{0.5}Sr_{0.5}Nb_2O_6/CoCr_{0.4}Fe_{1.6}O_4$ multiferroic composite that formed as a relaxor ferroelectric. Dalibor et al.[27] studied the dielectric properties as a function of frequency and temperature for MFe_2O_4 (M = Mn, Ni, Zn) ferrites. Panda et al.[25] reported on the frequency- and temperature-dependent dielectric permittivity of bulk cobalt ferrite, where relaxation frequency and grain and grain boundary contributions were found.

The magnetodielectric (MD) effect is the tendency of a material to change the value of its permittivity in an externally applied magnetic field. In recent years, researchers worldwide have devoted experimental and theoretical research efforts to investigating the MD effect due to its potential application in magnetic sensors, storage devices, and microwave resonators.[28–32] It is well known that the MD effect is attributed to hopping polarization and interface effects. In addition, the Maxwell–Wagner and magnetoresistance effects contribute to this effect. Oh et al.[28] reported an MD ratio of less than 0.5% induced by a magnetic field up to 9 T in $ErFeO_3$. Pan et al.[29] reported an MD ratio of Mn-Zn ferrite of 1.4% up to 4 T. In the extrinsic effect, grain and grain boundaries are important in improving the MD effect for ferrites at room temperature.

In this work, the surface morphology grain distribution of $Co_{1-x}Cr_xFe_2O_4$ ($x = 0$, 0.125, 0.25, 0.375, and 0.5) and the effect of Cr^{3+} substitution are studied, including a detailed investigation of the dielectric properties as a function of frequency and temperature. The behavior of ferroelectrics and the electric modulus are discussed. A detailed study of the MD effect is carried out by analyzing the magnetic field-dependent dielectric permittivity.

Experimental

The required amount of raw materials, including Co_2O_3 (98.0%), Cr_2O_3 (99.9%), and Fe_2O_3 (96.0%), were used to synthesize the nominal chemical compositions of $Co_{1-x}Cr_xFe_2O_4$ ($x = 0.000$, 0.125, 0.250, 0.375, and 0.500). All the raw materials for each composition were mixed in a mortar by a pestle for 2 h and then milled for 12 h on a planetary ball mill (MSK-SFM-1). To conduct a complete solid-state reaction, the milled powders were successively calcined at 800°C for 6 h, pelletized using a uniaxial pressure of 16,000 psi, and sintered at 1200°C for 6 h. Then, x-ray diffraction (XRD) was conducted on the re-crushed powder from a portion of the sintered pellets, and the single-phase spinel-type ferrite formation with space group Fd-3 m of sintered pellets was confirmed, as reported elsewhere.[21] The complex permittivity data were scanned for various frequencies, temperatures, and magnetic fields on the sintered pellets using a Wayne Kerr 6500B impedance analyzer.

Results and Discussion

Microstructure Analysis

The microstructure, including the shape, texture, and distribution of materials at a surface, can be analyzed by imaging the surface morphology, which provides evidence to explain the electrical properties. In this research article, we performed scanning electron microscopy (SEM) imaging, and the line intercept method was used to estimate the average grain size of Cr^{3+}-substituted CFO. The SEM micrographs for all the Cr^{3+} concentrations and the histograms are illustrated in Fig. 1. The SEM micrograph shows a dense structure with good grains, low porosity, and low agglomeration. For $x = 0.125$-0.375, clear grain and grain boundaries are evident, but for $x = 0$ and $x = 0.5$, less visible grain and grain boundaries are observed because, for these two samples, a tendency towards agglomeration has developed, which may be due to the moisture effect and magnetic interaction.[1] The average grain size obtained from the histograms (Fig. 1a, b, c, d, and e) reveals a micro size in the range of 0.98 μm–1.4 μm, which is much larger than the crystallite size (47–60 nm) as estimated from XRD.[21] The larger grain size is ascribed to the agglomeration of many crystallites in high-temperature sintering. With the increase of Cr^{3+} concentration, the average grain size exhibits a decreasing trend (Fig. 1f) due to the decreasing trend of crystallite size.[21] For $x = 0.5$, the average grain size is observed to be smaller than 1 μm with agglomeration, which is assumed to form due to centripetal force, where the cohesive van der Waals force plays a role as the bonding force holding these particles together within the agglomerates.[33]

Complex Dielectric Properties

Frequency Dependence

It is well known that polycrystalline materials exhibit dielectric behavior due to the contribution of interfacial (grain boundary) and hopping (within grains) polarization.[34] The frequency-dependent real and imaginary parts of dielectric properties provide insight into the interfacial and hopping polarization. For this reason, we investigated the real (ε') and imaginary (ε'') permittivity at room temperature as a function of frequency for all examined samples. The ε' versus frequency is illustrated in Fig. 2, where all samples exhibit higher ε' values at low frequency (100 Hz), which is due to the interfacial and dipolar polarization at the grain boundaries.[34] These higher values of ε' at low frequency generate a potential barrier and display

Fig. 1 (a) SEM micrographs for various Co$_{1-x}$Cr$_x$Fe$_2$O$_4$ (a) $x=0.0$, (b) $x=0.125$, (c) $x=0.250$, (d) $x=0.375$, and (e) $x=0.500$. (f) Grain size versus Cr concentration plots.

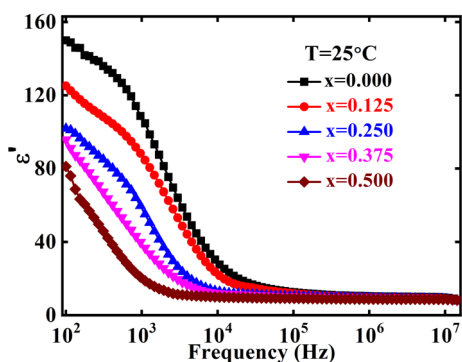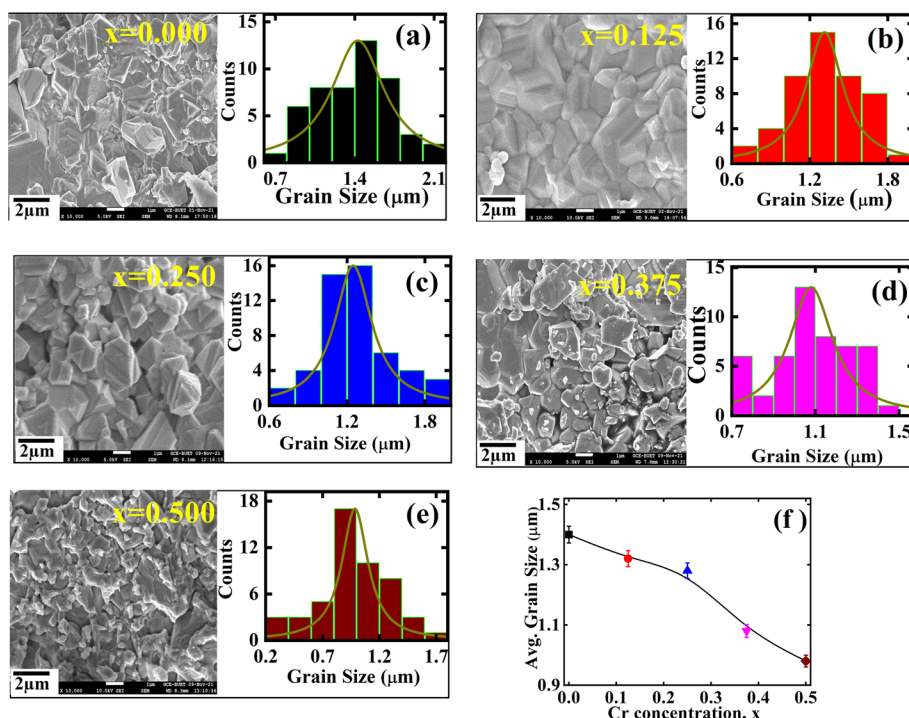**Fig. 2** The frequency dependence of the real part of the complex permittivity for various Co$_{1-x}$Cr$_x$Fe$_2$O$_4$.

Fig. 3 The frequency dependence of dielectric loss for various Co$_{1-x}$Cr$_x$Fe$_2$O$_4$.

inhomogeneous dielectric behavior. With the increased frequency, the interfacial polarization decreases, and hopping polarization develops at low resistive grains separated by poorly conducting thin grain boundaries. The reduction of interfacial polarization and development of ionic and electronic polarization decreases the ε' values for all samples as scanned in the frequency range of 100 Hz to 10 MHz (Fig. 2).

The dielectric loss (tan δ) obtained from the $\varepsilon''/\varepsilon'$ ratio represents the energy loss of dielectric materials that emerged from the space charge migration and movement of molecular dipoles.[34] In this research article, the tan δ values as a function of frequency are represented in Fig. 3. At low frequency, high resistive grain boundaries for all samples are more effective than grains with higher values of tan δ. The
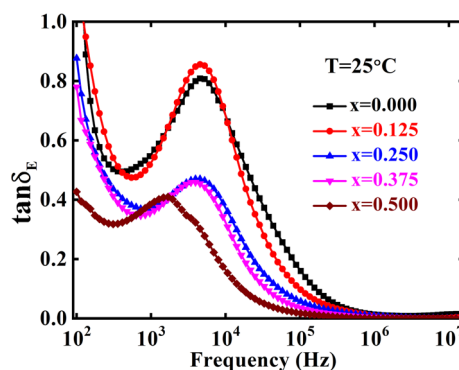
tan δ values show a decreasing trend and exhibit a peak value at a certain frequency which is due to the resonance behavior. After the peak value of tan δ, the values decrease continuously and approximately diminish in the high-frequency region, which may be attributed to the low resistive grains of the examined samples. From Figs. 2 and 3, it is demonstrated that the decreasing values of ε' and tan δ with the increase of Cr^{3+} is due to the decreasing grain size as explained in the section "Microstructure Analysis".

Temperature Dependence

The temperature (T)-dependent complex permittivity is measured for all samples at a high frequency of 1 MHz

Fig. 4 The temperature dependence of the real part of the complex permittivity (left axis) and the inverse of the real part of complex permittivity (right axis) for various $Co_{1-x}Cr_xFe_2O_4$; (a) $x = 0.0$, (b) $x = 0.125$, (c) $x = 0.25$, (d) $x = 0.375$, and (e) $x = 0.500$. (f) $Ln(1/\varepsilon' - 1/\varepsilon'_{max})$ versus $Ln(T - T_m)$ plots for various $Co_{1-x}Cr_xFe_2O_4$.
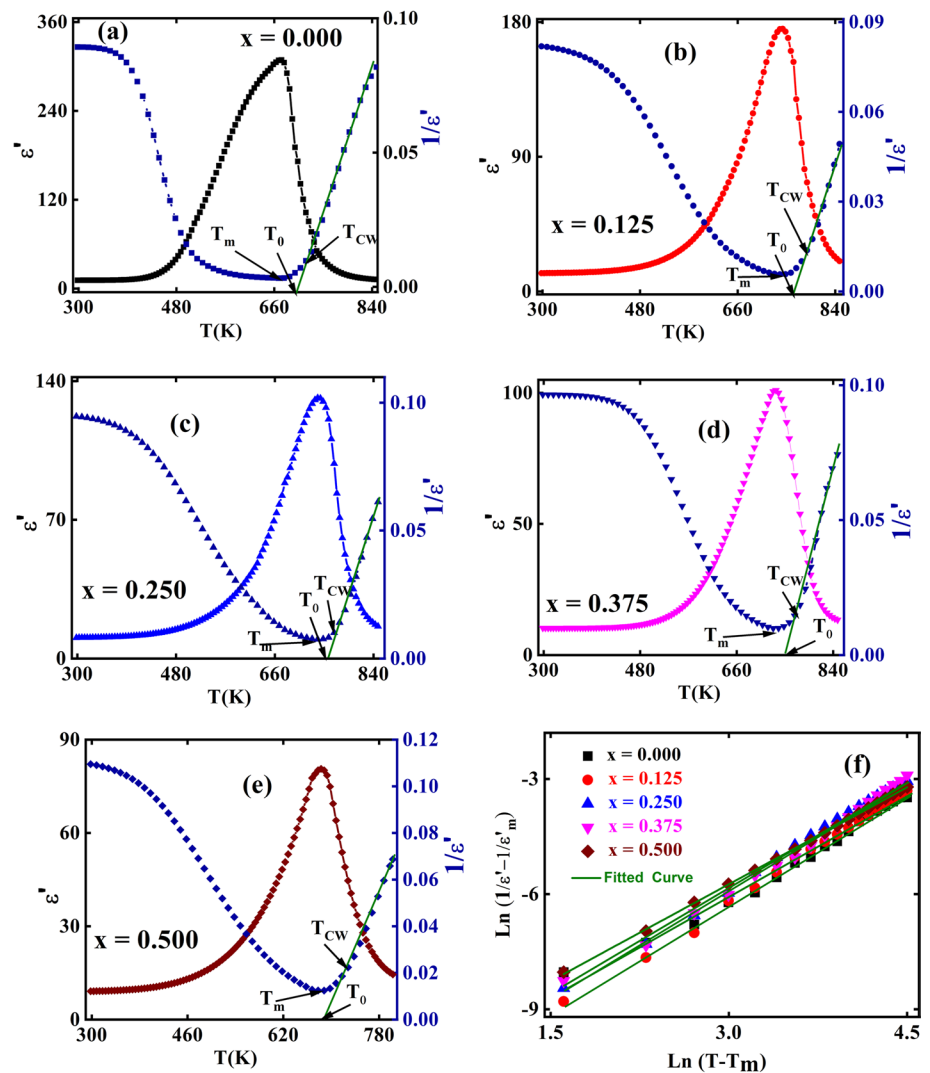
because, in the high-frequency region, the dielectric loss shows minimum values. Figure 4a, b, c, d, and e demonstrates the T versus ε' graph, where an increasing trend of ε' is found with increasing T for all samples due to thermally activated hopping charge carriers[26] From Fig. 4a, b, c, d, and e, the ε' values are found to increase up to 673 K, 743 K, 738 K, 728 K, and 688 K, respectively, for $x = 0.00$, $x = 0.125$, $x = 0.250$, $x = 0.375$, and $x = 0.500$, after which they fall rapidly. These maximum peak values of ε' indicate the ferroelectric to paraelectric transition temperature[26,35], which is close to the magnetic phase transition temperature as explained in a previously reported article.[22] The dielectric phenomenon in all samples can be explained by plotting the $1/\varepsilon'$ versus T (Fig. 4a, b, c, d, and e) according to the Curie-Weiss law given as follows[35]:

$$\frac{1}{\varepsilon'} = \frac{T - T_0}{C} \tag{1}$$

Here, C is the Curie constant and T_0 is the Curie-Weiss temperature. From Fig. 4 it is observed that the ε' values of all samples deviate from the Curie-Weiss Law above the Curie temperature. To explain these deviations, the following expression is developed[36]

$$\Delta T_m = T_{CW} - T_m \tag{2}$$

Here, ΔT_m denotes the degree of deviation, T_m denotes the temperature at which the ε' value reaches the maximum, and T_{CW} represents the temperature from which it starts to deviate from the Curie–Weiss law. The linear fit of $1/\varepsilon'$ versus T (Fig. 4a and b) above T_C for all samples gives the parameters C, T_0, and T_{CW}, which are listed in Table I. The T_m and ΔT_m and maximum real permittivity (ε'_{max}) at 1 MHz obtained from Fig. 4 are presented in Table I. From Table I, the C and T_0 values are found to correspond to the Curie-Weiss behavior of the inverse dc susceptibility graph as explained in a previously

Table I Curie Weiss temperature (T_0) and temperature (T_m) at maximum ε' value, start of deviated temperature (T_{CW}), deviation of temperature ΔT_m (K), Curie constant (C), and diffuseness coefficient (γ)

x	T_m, K	T_{CW}, K	T_0, K	ΔT_m, K	C	γ
0.000	673	719	700	46	1754	1.70
0.125	743	783	762	40	2000	1.95
0.250	738	775	752	37	1961	1.93
0.375	728	762	748	34	1613	1.92
0.500	688	688	688	31	1703	1.68

published article.[22] In addition, the ΔT_m was found to decrease with increasing Cr^{3+} concentration, which indicates a diffuse phase transition that is enhanced by the decrease in grain size as explained in the section "Microstructure Analysis". It is well known that the Curie-Weiss law (Eq. 1) is applicable for the sharp permittivity peak[35] at around T_m. Since no sample in the present study shows a sharp permittivity peak, a modified Curie-Weiss law (Eq. 3), first proposed by Uchino and Nomura,[36] has been employed.

$$\frac{1}{\varepsilon'} - \frac{1}{\varepsilon'_{max}} = \frac{(T - T_m)^\gamma}{C} \quad (3)$$

Here, γ is the diffuseness coefficient which shows the character of the phase transition.[37] $\gamma = 1$ signifies the ideal Curie-Weiss law from which a clear concept of classical transition of ferroelectric materials can be understood. γ values in the range of $1 < \gamma < 2$ signify the diffuse transition, and a clear concept of an ideal relaxor ferroelectric can be known to form γ values equal to 2.[38] The $Ln(1/\varepsilon' - 1/\varepsilon'_{max})$ versus $Ln(T - T_m)$ graphs for all samples are illustrated in Fig. 4f, where the slope of linear fit of the curves provide the γ values that are listed in Table I. From Table I it is clear that the γ values for $x = 0.125$, 0.250, and 0.375 are very close to 2, which indicates that these three samples are relaxor ferroelectric compounds. However, $x = 0.00$ and 0.50 samples behave as defuse ferroelectrics, which is due to the γ values between 1 and 2. The room-temperature dielectric loss as a function of frequency shows a high loss at low frequencies, but it shows much lower values at high frequencies. However, the imaginary part of complex permittivity (ε'') as a function of T shows the same behavior as the dielectric constant for all the samples, as demonstrated in Fig. 5. From Fig. 5 it is found that the ε'' values show a maximum at around transition temperature which is due to the charge accumulation at grain boundaries.[39]

Electric Modulus Analysis

The dielectric relaxation of a compound can be analyzed by studying the complex electric modulus [$M^*(\omega)$] as formulated by the following equation[40]:
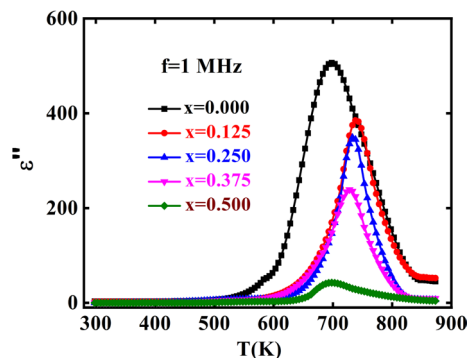

Fig. 5 The temperature dependence of the imaginary part of the complex permittivity for various $Co_{1-x}Cr_xFe_2O_4$.

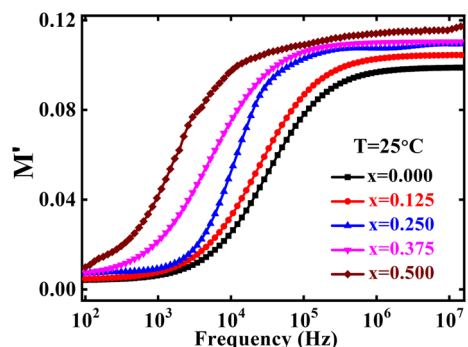**Fig. 6** The frequency dependence of the real part of electric modulus for various $Co_{1-x}Cr_xFe_2O_4$.

$$[M^*(\omega)] = \frac{1}{\varepsilon^*} = \frac{1}{\varepsilon' - j\varepsilon''} = \frac{\varepsilon'}{\varepsilon'^2 + \varepsilon''^2} + j\frac{\varepsilon''}{\varepsilon'^2 + \varepsilon''^2} = M' + jM'' \quad (4)$$

where $M' = \frac{\varepsilon'}{\varepsilon'^2 + \varepsilon''^2}$ and $M'' = \frac{\varepsilon''}{\varepsilon'^2 + \varepsilon''^2}$ are the real and imaginary parts of the electric modulus.

The calculation of frequency-dependent real (M') and imaginary (M'') electric modulus can be used to find the relaxation process. The M' versus frequency plot for all samples is illustrated in Fig. 6, where M' values show an increasing trend in the low-frequency region which is due to the short-range mobility of charge carriers. However, at the high-frequency region, it shows saturation when reaching the maximum M' values, which is known as the plateau
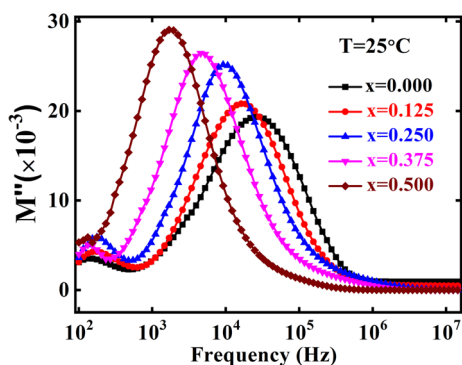
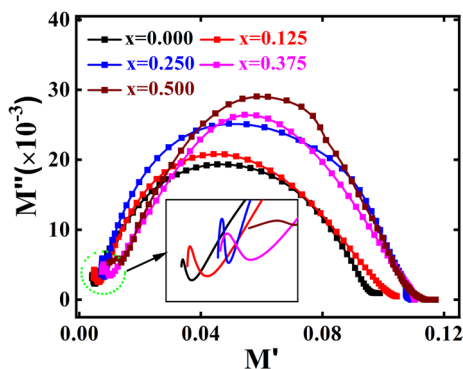**Fig. 7** The frequency dependence of imaginary part of electric modulus for various $Co_{1-x}Cr_xFe_2O_4$.

Fig. 8 M'' versus M' plots for various $Co_{1-x}Cr_xFe_2O_4$.

region, indicating the relaxation process.[40] From Fig. 6 it is seen that the starting point in the plateau region shifts towards low frequency with the increase of Cr^{3+}, which is due to the decrease of grain size. Figure 7 demonstrates the imaginary part of the electric modulus (M'') as a function of frequency where two peaks in each concentration have been found, one of which is at low frequency and the other is at high frequency. From Fig. 7 is seen that both peaks shift towards the low frequency region with the increase of Cr^{3+} concentration originating from the decrease in hopping length as explained by Jing et al.[13] The M'' versus M' curves for all samples are plotted in Fig. 8, where two semicircular arcs are found, one of which is at low frequency and the other is at high frequency. The two semicircles correspond to the synthesized samples and behave as two types of relaxation. The grain boundaries contribute to the small semicircle at low frequency where the grains/bulk response has been dominated by another large semicircle at the high-frequency region.

Magnetodielectric Analysis

The MD effect is the magnetic response on dielectric properties of a material that can be estimated by using the following equation[41]:

$$MD(\%) = \frac{\varepsilon(H) - \varepsilon(0)}{\varepsilon(0)} \times 100 \qquad (5)$$

where $\varepsilon(H)$ and $\varepsilon(0)$ represent the dielectric constant at the applied magnetic field and zero magnetic field, respectively. The MD (%) versus f graphs are presented in Fig. 9a, b, and c, respectively, for 0.1 T, 0.5 T, and 1.0 T, where at 0.1 T a lower MD (%) with a chaotic curve is evident for all samples. However, at 0.5 T and 1.0 T, MD (%) is found to have a larger value, and the smoothness of the MD (%) versus f curve that develops indicates that the applied magnetic fields are responsible for the change in dielectric constant. From Fig. 9c, MD (%) shows an obvious peak value at around a certain frequency for all samples, corresponding to the relaxation frequency as evident from the section 3.3. At around the relaxation frequency, the MD effect is induced by hopping polarization and an interface effect which is ascribed to the most intense peak of MD (%) which is combined with the Maxwell-Wagner effect. In addition, the spin-phonon coupling is the possible cause behind the most intense peak for the MD effect at around the relaxation frequency.[28] From Fig. 9c the shifts of the most intense peak of MD (%) towards the optical phonon frequency with an increase of Cr^{3+} content have been found which may be induced by spin-spin correlation and interaction of Co^{2+}-Cr^{3+}. After the relaxation peak, the MD (%) decreases rapidly and almost no MD effect has been shown in high-frequency regions. MD (%) as a function of the magnetic field has been illustrated in Fig. 9d where an increasing trend of MD (%) with the increase in magnetic field has been found. The maximum MD (%) is found to be in the range of (2.5–6.5%) for 1 T which is much larger than the previously reported data[29,32] indicating a potential divergence in the observed methodology used in the study. The enhancement of MD (%) with the increase of magnetic field may arise due to the magnetic ordering that corresponds to the magnetic moment as described in detail in the previously published article. The applied magnetic field causes the force alignment of Fe^{2+} and Fe^{3+} ions distributed into the tetrahedral and octahedral site[21] decreasing the scattering of charges and promoting Fe^{2+}-Fe^{3+} dipoles which results in the positive MD effect. From Fig. 9d it is observed that the MD (%) decreases with the increase of Cr^{3+} content. As the saturation magnetization decreases within Cr^{3+} it results in the drop-down of MD (%).[22] Abnormal grain growth and pore blockage due to a larger ratio of Cr^{2+}/Co^{2+} at tetrahedral sites compared

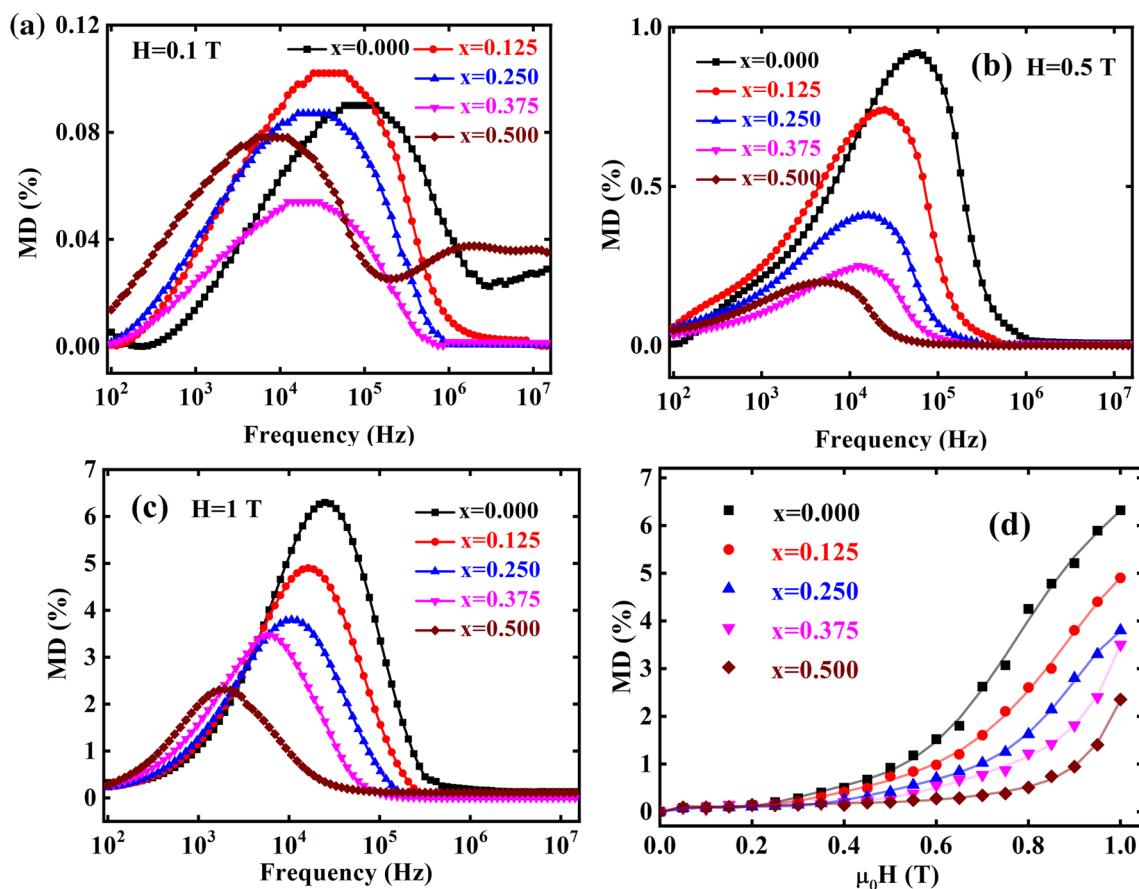**Fig. 9** The frequency dependence of MD % for various $Co_{1-x}Cr_xFe_2O_4$ (a) for 0.1 T, (b) 0.5 T, (c) 1 T, (d) MD (%) versus H plots for various $Co_{1-x}Cr_xFe_2O_4$.

to Cr^{3+}/Co^{2+} at octahedral sites might reduce the magnetic moment, increase charge scattering, and lower MD (%).

Conclusions

The $Co_{1-x}Cr_xFe_2O_4$ ($x=0.0$, 0.125, 0.250, 0.375, and 0.500) compounds, with Fd-3 m space group of the cubic system, have been synthesized by solid-state reaction via ball milling. The Cr^{3+} substitution with cobalt ferrite reduces the permittivity as corresponds to the average grain size. The existence of a ferro/paraelectric phase transition around magnetic phase transition has been established by the dielectric measurements. The empirical parameter γ indicates that the compounds for $x=0.125$, 0.250, and 0.375 are the relaxor ferroelectric, which is expected to be applicable for high-efficiency energy storage and conversion. However, the compounds for $x=0.00$ and 0.50 are diffuse ferroelectric, which is suggested to be applicable to electrocaloric cooling systems. All synthesized samples dominate grain boundary and grain response, respectively, at low- and high-frequency regions. The existence of large MD (%) at around

the relaxation frequency has been observed from the dielectric measurements. Cr^{3+} substitution plays a vital role in decreasing MD (%), which corresponds to saturation magnetization. Based on these findings, Cr^{3+}-substituted cobalt ferrite appears to be a promising candidate for multifunctional device applications.

Conflict of interest The authors declare that they have no conflict of interest.

References

1. J. Massoudi, M. Smari, K. Nouri, E. Dhahri, K. Khirouni, S. Bertaina, and L. Bessais, Magnetic and spectroscopic properties of Ni-Zn-Al ferrite spinel: from the nanoscale to microscale. *RSC Adv.* 10(57), 34556–34580 (2020).
2. N. Amri, J. Massoudi, K. Nouri, M. Triki, E. Dhahri, L. Bessais, and L., Influence of neodymium substitution on structural,

magnetic, and spectroscopic properties of Ni-Zn-Al nano-ferrites. *RSC Adv.* 11(22), 13256–13268 (2021).

3. H.Q. Alijani, S. Iravani, S. Pourseyedi, M. Torkzadeh-Mahani, M. Barani, and M. Khatami, Biosynthesis of spinel nickel ferrite nanowhiskers and their biomedical applications. *Sci. Rep.* 11(1), 17431 (2021).

4. N. Kouki, S. Hcini, M. Boudard, R. Aldawas, and A. Dhahri, Microstructural analysis, magnetic properties, magnetocaloric effect, and critical behaviors of $Ni_{0.6}Cd_{0.2}Cu_{0.2}Fe_2O_4$ ferrites prepared using the sol–gel method under different sintering temperatures. *RSC Adv.* 9(4), 1990–2001 (2019).

5. A. Spivakov, C. Lin, E. Lin, Y. Chen, and Y. Tseng, Preparation and magnetic properties of cobalt-doped $FeMn_2O_4$ spinel nano-particles. *Nanoscale Res. Lett.* 16, 162 (2021).

6. S.K. Gore, S.S. Jadhav, V.V. Jadhav, S.M. Patange, M. Naushad, R.S. Mane, and K.H. Kim, The structural and magnetic properties of dual phase cobalt ferrite. *Sci. Rep.* 7(1), 2524 (2017).

7. M.A. Almessiere, Y. Slimani, H. Güngüneş, S. Ali, A. Manikan-dan, I. Ercan, A. Baykal, and A.V. Trukhanov, Magnetic attributes of $NiFe_2O_4$ nanoparticles: influence of dysprosium ions (Dy^{3+}) substitution. *Nanomater.* 9(6), 820 (2019).

8. R. Lahouli, J. Massoudi, M. Smari, H. Rahmouni, K. Khirouni, E. Dhahri, and L. Bessais, Investigation of annealing effects on the physical properties of $Ni_{0.6}Zn_{0.4}Fe_{1.5}Al_{0.5}O_4$ ferrite. *RSC Adv.* 9(35), 19949–19964 (2019).

9. S.U. Rather, H.S. Bamufleh, and H. Alhumade, Structural, thermal, morphological, surface, chemical, and magnetic analysis of Al^{3+}-doped nanostructured mixed-spinel cobalt ferrites. *Ceram. Int.* 47(12), 17361–17372 (2021).

10. P. Bera, R.V. Lakshmi, B.H. Prakash, K. Tiwari, A. Shukla, A.K. Kundu, K. Biswas, and H. Barshilia, Solution combustion synthesis, characterization, magnetic, and dielectric properties of $CoFe_2O_4$ and $Co_{0.5}M_{0.5}Fe_2O_4$ (M = Mn, Ni, and Zn). *Phys. Chem. Chem. Phys.* 22, 20087–20106 (2020).

11. C. Aziz and B. Azhdar, Synthesis of dysprosium doped cobalt ferrites nanoparticles by sol-gel auto-combustion method and influence of grinding techniques on structural, morphological, and magnetic properties. *J. Magn. Magn* 542, 168577 (2022).

12. X. Qin, T. Zhang, J. Wang, R. Zhao, Y. Ma, F. Fang Wang, and X. Xu, Influence of Ce-Mn co-doping on the structure and magnetic properties of cobalt ferrites. *J. Alloys Compd.* 929, 167256 (2022).

13. X. Jing, M. Guo, Z. Li, C. Qin, Z. Chen, Z. Li, and H. Gong, Study on structure and magnetic properties of rare earth doped cobalt ferrite: The influence mechanism of different substitution positions. *Ceram. Int.* 49(7A), 14046–14056 (2023).

14. A.A. Ati, A.H. Abdalsalam, and A.S. Hasan, Thermal, microstructural and magnetic properties of manganese substitution cobalt ferrite prepared via co-precipitation method. *J. Mater. Sci. Mater. Electron.* 32(3), 3019–3037 (2021).

15. D. Karthickraja, S. Karthi, G.A. Kumar, D.K. Sardar, G.C. Dannangoda, K.S. Martirosyan, and E.K. Girija, Fabrication of core–shell $CoFe_2O_4$@ HAp nanoparticles: a novel magnetic platform for biomedical applications. *New J. Chem.* 43(34), 13584–13593 (2019).

16. M.Z. Ahsan, F.A. Khan, and M.A. Islam, Frequency and temperature dependent dielectric and magnetic properties of manganese doped cobalt ferrite nanoparticles. *J. Electron. Mater.* 48, 7721–7729 (2019).

17. M.Z. Ahsan, F.A. Khan, and M.A. Islam, Frequency and temperature dependent intrinsic electric properties of manganese doped cobalt ferrite nanoparticles. *Res. Phys.* 14, 102484 (2019).

18. Y. Slimani, M.A. Almessiere, S. Guner, B. Aktas, S.E. Shirsath, M.V. Silibin, A.V. Trukhanov, and A. Baykal, Impact of Sm^{3+} and Er^{3+} cations on the structural, optical, and magnetic traits of spinel cobalt ferrite nanoparticles: comparison investigation. *ACS Omega* 7, 6292–6301 (2022).

19. D. Thomas, I.G. Deac, C. Oana, E.A. Levei, L. Diamandescu, and G. Borodi, Effect of Zn content on structural, morphological, and magnetic behavior of $Zn_xCo_{1-x}Fe_2O_4/SiO_2$ nanocomposites. *J. Alloy. Compd.* 792, 432–443 (2019).

20. S. Jauhar, J. Kaur, A. Goyal, and S. Singhal, Tuning the properties of cobalt ferrite: a road towards diverse applications. *RSC Adv.* 6(100), 97694–97719 (2019).

21. M.A. Islam, A.K.M. Akther Hossain, M.Z. Ahsan, M.A.A. Bally, M. Samir Ullah, S.M. Hoque, and F.A. Khan, Structural characteristics, cation distribution, and elastic properties of Cr^{3+} substituted stoichiometric and non-stoichiometric cobalt ferrites. *RSC Adv.* 12, 8502–8519 (2022).

22. M.A. Islam and A.K.M. Akther Hossain, Magnetic properties, magnetocaloric effect, and critical behaviors in $Co_{1-x}Cr_xFe_2O_4$. *RSC Adv.* 12, 17362–17378 (2022).

23. G.A. Lone and M. Ikram, Investigating the structural and dielectric properties of $CoFe_{2-x}Ni_xO_4$ spinel ferrite. *J. Alloys Compd.* 5(908), 164589 (2022).

24. A. Kumar, P. Sharma, and D. Varshney, Structural, vibrational, and dielectric study of Ni-doped spinel Co ferrites: $Co_{1-x}Ni_xFe_2O_4$ (x=00, 05, 10). *Ceram. Int.* 40(8), 12855–12860 (2014).

25. R.K. Panda and D. Behera, Investigation of electric transport behavior of bulk $CoFe_2O_4$ by complex impedance spectroscopy. *J. Alloys Compd.* 587, 481–486 (2014).

26. S. Tiwari and S. Vitta, Magnetoelectric and magnetodielectric coupling and microwave resonator characteristics of $Ba_{0.5}Sr_{0.5}Nb_2O_6/CoCr_{0.4}Fe_{1.6}O_4$ multiferroic composite. *Sci. Rep.* 8(1), 11619 (2018).

27. D.L. Sekulic, Z.Z. Lazarevic, M.V. Sataric, C.D. Jovalekic, and N.Z. Romcevic, Temperature-dependent complex impedance, electrical conductivity, and dielectric studies of MFe_2O_4 (M = Mn, Ni, Zn) ferrites prepared by sintering of mechanochemical synthesized nanopowders. *J. Mater. Sci. Mater. Electron.* 26(3), 1291–1303 (2015).

28. J.F. Scott, Data storage: multiferroic memories. *Nat. Mater.* 6(4), 256–257 (2007).

29. P. Pan, and N. Zhang, Hysteresis behavior of the magnetodielectric effect in Mn-Zn Ferrite. *Phys. Status Solidi B* 255(6), 1700551 (2018).

30. F. Chen, X. Wang, Y. Nie, Q. Li, J. Ouyang, Z. Feng, Y. Chen, and V.G. Harris, Ferromagnetic resonance induced a large microwave magnetodielectric effect in cerium-doped $Y_3Fe_5O_{12}$ ferrites. *Sci. Rep.* 6, 28206 (2016).

31. T. Basu, A. Pautrat, V. Hardy, A. Loidl, and S. Krohns, Magnetodielectric coupling in a Ru-based 6H-perovskite, $Ba_3NdRu_2O_9$. *Appl. Phys. Lett.* 113(4), 042902 (2018).

32. D.G. Oh, J.H. Kim, H.J. Shin, Y.J. Choi, and N. Lee, Anisotropic and nonlinear magnetodielectric effects in orthoferrite $ErFeO_3$ single crystals. *Sci. Rep.* 10(1), 11825 (2020).

33. R.Y. Yang, A.B. Yu, S.K. Choi, M.S. Coates, and H.K. Chan, Agglomeration of fine particles subjected to centripetal compaction. *Powder Technol.* 184(1), 122–129 (2008).

34. B.D. Lakshmi, K. Pratap, B.P. Rao, and P.S.V.S. Rao, Impedance spectroscopy and dielectric properties of multiferroic $BiFeO_3/Bi_{0.95}Mn_{0.05}FeO_3–Ni_{0.5}Zn_{0.5}Fe_2O_4$ composites. *Ceram. Int.* 42(2A), 2186–2197 (2016).

35. F. HuiQing and K.E. ShanMing, Relaxor behavior and electrical properties of high dielectric constant materials. *Sci. China Ser. Eng. Tech. Sci.* 8, 2180–2185 (2009).

36. K. Uchino and N. Shoichiro, Critical exponents of the dielectric constants in diffused-phase-transition crystals. *Ferroelectrics* 44(1), 55–61 (1982).

37. C. Rayssi, S.E. Kossi, J. Dhahri, and K. Khirouni, Frequency and temperature-dependence of dielectric permittivity and electric

modulus studies of the solid solution $Ca_{0.85}Er_{0.1}Ti_{1-x}Co_{4x/3}O_3$ ($0 \leq x \leq 0.1$). *Rsc Adv.* 8(31), 17139–17150 (2018).

38. X. Wang and H. Chen, Dielectric behaviors under high electric field for $Pb(Zr_{1/3}Nb_{2/3})O_3$-$PbTiO_3$-$BaTiO_3$ relaxor ferroelectric ceramics. *J. Appl. Phys.* 91, 5979 (2002).

39. P.R. Das, L. Biswal, B. Behera, and R.N. Choudhary, Structural and electrical properties of $Na_2Pb_2Eu_2W_2Ti_4X_4O_{30}$ (X= Nb, Ta) ferroelectric ceramics. *Mater. Res. Bull.* 44(6), 1214–1218 (2009).

40. L. Patro and K. Hariharan, AC conductivity and scaling studies of polycrystalline SnF_2. *Mater. Chem. Phys.* 116, 81–87 (2009).

41. C. Vázquez-Vázquez, M. Lovelle, C. Mateo, M.A. López-Quintela, M.C. Buján-Núñez, D. Serantes, D. Baldomir, and J. Rivas, Magnetocaloric effect and size-dependent study of the magnetic properties of cobalt ferrite nanoparticles prepared by solvothermal synthesis. *Phys. Status Solidi A* 205(6), 1358–1362 (2008).